applied sciences

MDPI

Article

Study on the Energy Evolution Law of Sandstone and Its Implications for Rockburst Prevention Considering Particle Effect Under Thermal Action

Tianbin Li [1], Shuhao Qiu [1], Mengting Han [2], Ruichi Chang [2], Feng Zeng [1,2], Yan Zhang [1] and Meiben Gao [3,*]

[1] State Key Laboratory of Geohazard Prevention and Geoenvironment Protection, Chengdu University of Technology, Chengdu 610059, China
[2] School of Emergency Management, Xihua University, Chengdu 610039, China
[3] Key Laboratory of Landslide Risk Early-Warning and Control, Ministry of Emergency Management, Chengdu University of Technology, Chengdu 610059, China
* Correspondence: gaomb@mail.xhu.edu.cn

Abstract

Rockburst is one of the major geological hazards in the construction of deep-buried and high-geotemperature tunnels. Using triaxial compression tests and acoustic emission (AE) techniques, this paper conducts a preliminary exploratory investigation on the deformation and failure characteristics, mechanical parameters, acoustic emission responses and energy evolution laws of typical rockburst-prone rocks under confining pressures of 10–30 MPa and temperatures of 100–250 °C. The results show that within the research scope, sandstone exhibits brittle characteristics including compaction, linear elasticity, crack initiation and propagation, stable crack propagation stage, accelerated crack propagation stage, and stress drop stage. Within a certain range, peak strength and damage strength increase with the rise in confining pressure and temperature. The elastic modulus increases with rising confining pressure. The damage point may be the critical point of energy conversion and acoustic emission activity. After damage, the work done by external forces is mainly converted into dissipated energy. With the intensification of surrounding rock damage, the ratio of elastic strain energy to total energy gradually decreases, while the ratio of dissipated energy to total energy gradually increases. Acoustic emission activity increases significantly at the damage point and reaches its peak at the peak strength. The cumulative acoustic emission ring count and cumulative energy increase slowly before the peak and grow rapidly after the peak. Under thermo-mechanical action, new cracks in sandstone preferentially initiate along grain boundaries, and the inconsistent deformation between grains will promote the formation of transgranular cracks. The connection, convergence and final penetration of cracks lead to sample failure. The elevation of temperature and confining pressure can enhance the bearing capacity of sandstone, indicating that a high-temperature and high-stress environment may be conducive to the occurrence of rockbursts. The research results provide scientific support for an in-depth understanding of the mechanical behavior and instability risk of rockburst in deep-buried and high-geotemperature tunnels, and can provide a theoretical basis for rockburst prevention and control of high-geotemperature tunnels of the CZ Railway.

Keywords: sandstone; energy evolution; particle effect; triaxial compression test; rockburst

Check for updates

Received: 25 April 2026
Revised: 28 May 2026
Accepted: 2 June 2026
Published: 9 June 2026

Copyright: © 2026 by the authors. Licensee MDPI, Basel, Switzerland. This article is an open access article distributed under the terms and conditions of the Creative Commons Attribution (CC BY) license.

1. Introduction

With the rapid advancement of deep underground space development, the risk of rockburst in deep-buried tunnels under high-geotemperature and high-stress environments has increased significantly [1]. As a typical high in situ stress geological hazard, rockburst is accompanied by the release of intense energy, posing a serious threat to tunnel construction safety. According to the definition of rockburst disaster, its essence is a phenomenon in which the surrounding rock releases accumulated elastic strain energy, leading to sudden damage and ejection of the rock mass [2]. The surrounding rock of deep-buried tunnels is often in a three-dimensional unequal stress state, and high geotemperature environments are widely present in deep structural zones and high geothermal flux areas. The mechanical behavior of rock masses under such thermal environments is extremely complex. High-geotemperature tunnels are generally divided into dry-heat and wet-heat environments. A large number of engineering cases have revealed that under dry-heat environments, adverse phenomena such as spalling and cracking of sandstone tunnel surrounding rock and initial support are prominent (Figure 1a,b). Sandstone is a typical sedimentary rock widely distributed on land and seabed, composed of quartz, feldspar and other fine-grained minerals, with grains generally ranging from 0.063 to 2 mm. The connection and structural characteristics between these grains endow sandstone with a certain degree of strength and stability, forming unique brittle fracture and energy evolution characteristics. Its special structure and texture make it prone to disasters such as collapse and rockburst in deep tunnel engineering (Figure 1c,d) [3,4]. For example, in the YK53+908–YK53+912 section of Gaoloushan Tunnel on WJ Expressway, a blasting-induced impact rockburst occurred in the sandstone stratum (Figure 1d). After the blasting, clear rock fracture sounds were heard, followed by large-area ejection and collapse at the vault and the haunches on both sides [4]. Therefore, understanding the mechanical characteristics, energy evolution law and particle effect of sandstone under dry-heat environments is very important for predicting and preventing rockbursts in deep-buried and high-geotemperature tunnels.

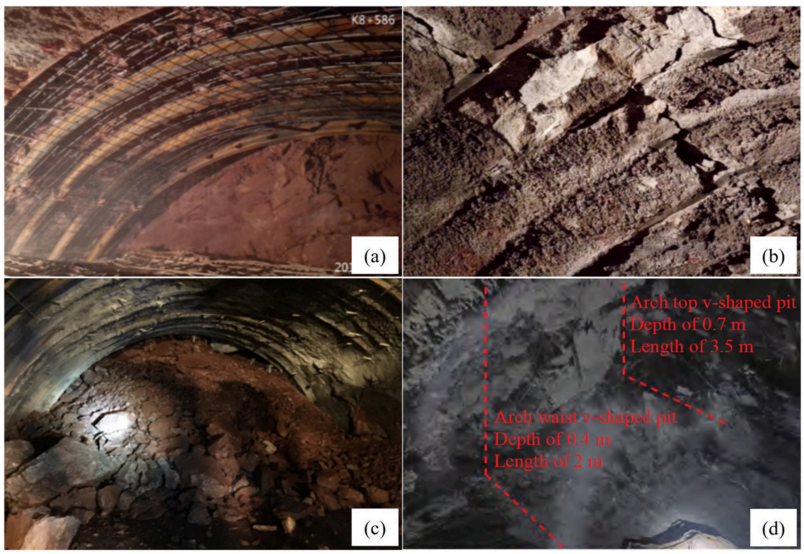

Figure 1. Typical adverse geological phenomena in sandstone stratum tunnels. (**a**) Sandstone tunnel. (**b**) Spalling of primary support. (**c**) Collapse. (**d**) Rockburst. Adapted from Ref. [4].

Numerous experimental studies have shown that high temperature exerts a significant influence on the mechanical parameters of sandstone, such as elastic modulus, strength, and peak strain. After high-temperature treatment or under real high-temperature conditions, the elastic modulus of sandstone generally tends to increase initially and then decrease

with a further rise in temperature, which is related to microscopic mechanisms such as pore closure/propagation and thermal expansion of minerals [5]. In high-temperature triaxial tests, the variation relationship between elastic modulus and temperature also depends on the confining condition and temperature range [6]. Further in situ high-temperature triaxial compression tests have shown that under high-temperature conditions, the changes in sandstone parameters such as peak strength, elastic modulus, and Poisson's ratio with temperature and confining pressure have complex nonlinear relationships [7]. In real high-temperature environments, the increase in temperature is usually accompanied by thermal damage and physical structure changes, which in turn lead to the transformation of elastic parameters and failure modes [8]. Traditional uniaxial tests cannot fully simulate the three-dimensional stress state of real underground surrounding rock, while triaxial tests can more truly reflect the mechanical response of deep rock masses under in situ stress conditions, including indicators such as peak strength, fracture angle, and deformation modulus [9]. True triaxial tests have shown that under the coupling effect of high temperature and high in situ stress, both the shear failure and brittle failure modes of sandstone are significantly affected, and the temperature and normal stress jointly determine the critical failure conditions. In addition, triaxial cyclic loading/unloading tests have revealed that under different intermediate principal stress conditions, the energy absorption and dissipation behaviors of sandstone show complex changes, reflecting the energy evolution law of microcrack initiation, propagation, connection and macroscopic failure [10].

In the field of rockburst research, the energy evolution theory has become an important framework for explaining the mechanism of rockburst occurrence. Essentially, a rockburst is a sudden imbalance in the process of energy storage, release and transfer of surrounding rock [11]. Studies based on true triaxial rapid unloading tests have shown that the more elastic strain energy accumulates and the higher the energy release rate, the higher the rockburst intensity, and the release process is accompanied by a large number of acoustic emission events and crack penetration [2]. Studies have also found that different rock masses, loading paths and unloading rates can lead to differences in the energy evolution characteristics and failure modes of rockburst; for example, there are obvious differences in the energy distribution and crack modes between delayed rockburst and instantaneous rockburst [12].

Although numerous studies have explored the mechanical parameters, elastic modulus and failure modes of rocks under high-temperature and high-stress conditions, most of them focus on the high-temperature range from room temperature to 600–1000 °C. Relatively few investigations have been carried out on small-gradient temperature differences within the engineering temperature range (room temperature to 250 °C), and studies concerning the temperature effect on rockbursts are even more scarce. Therefore, based on triaxial loading tests, this paper firstly studies the mechanical behaviors, AE energy evolution, particle effects and thermal effects of sandstone in dry thermal environments. Then, it was found that an increase in temperature and confining pressure could enhance the bearing capacity of sandstone, indicating that a high-temperature and high-pressure environment might be conducive to the occurrence of rockbursts.

2. Test Introduction

2.1. Test Apparatus

The tests were carried out using the IRSM-THM-1500 multi-field coupling testing system (Figure 2) from the Experimental Center of the School of Emergency Management, Xihua University. The IRSM-THM-1500 testing equipment was developed by the Institute of Rock and Soil Mechanics, Chinese Academy of Sciences, Wuhan, China. This apparatus can perform mechanical tests on rock specimens under thermo-hydro-mechanical (THM)

coupling conditions, including uniaxial compression, triaxial compression, creep, and stress relaxation tests. The system has a frame stiffness of 8 MN/mm, a maximum axial load of 150 tons, a maximum confining pressure of 60 MPa, and an operating temperature range from room temperature to 95 °C. The test system is equipped with a muffle furnace and acoustic emission (AE) equipment, enabling real-time monitoring of acoustic emission signals during the tests.

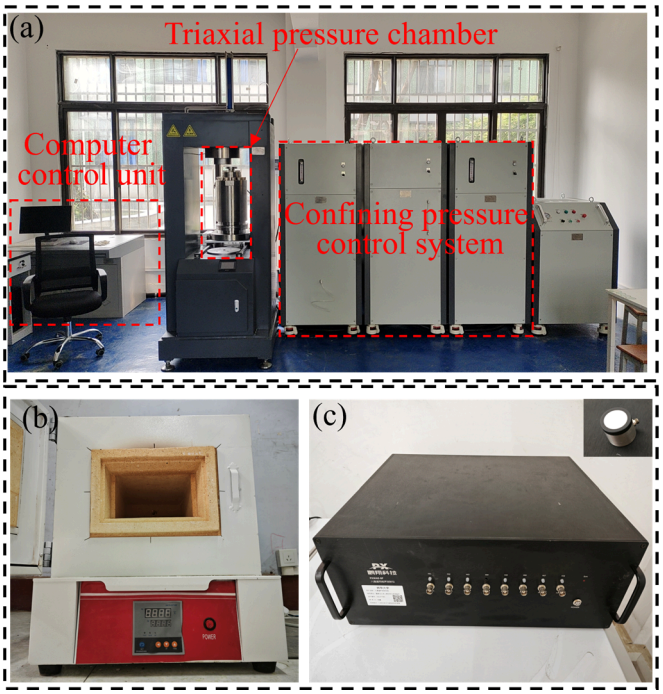

Figure 2. IRSM-THM-1500 multi-field coupling testing system. (**a**) RSM-THM-1500 testing equipment. (**b**) Muffle furnace. (**c**) Acoustic Emission testing system.

2.2. Test Scheme

The sandstone specimens used in this test were collected from Kangding, Sichuan Province, which belongs to the Southern Xizang–Western Sichuan–Western Yunnan geothermal active intensive zone. The main temperature in this area is 150 °C, and the burial depth of 1000–3000 m is a typical interval for high geotemperature occurrence. Therefore, four temperature levels (100 °C, 150 °C, 180 °C, 250 °C) and three confining pressure levels (10 MPa, 20 MPa, 30 MPa) were set. First, the mechanical characteristics and energy evolution law of sandstone at 150 °C under different confining pressures were analyzed, followed by those at 30 MPa under different temperatures. The detailed experimental scheme is shown in Table 1. The sandstone is yellowish-white in color, with an average density of 2.09 g/cm^3 and a natural water content of 0.94% (Table 1). In accordance with the standard for engineering rock mass test methods, the rock blocks were processed into standard cylindrical specimens with a diameter of 50 mm and a height of 100 mm (Table 1).

To further identify its mineral composition and particle size distribution, X-ray diffraction tests and polarized microscope observations of rock thin sections were carried out. The results show that the sandstone used in this study is dominated by quartz, accounting for 53%, followed by calcite at 16%, plagioclase at 14%, and clay minerals (illite, chlorite) at 17% (Table 2). Thin section observations indicate that the sandstone exhibits a fine-grained texture, mainly composed of mineral clastics such as quartz and feldspar, rock clastics such as limestone and siliceous rocks, as well as interstitial materials. The cement is mainly distributed among clastic particles with relatively uniform distribution.

Table 1. Sandstone specimens and experimental scheme.

No.	Mass/g (Before Heating)	Mass/g (After Heating)	Mass Loss Rate/%	Volume/cm^3	Initial Density/g·cm^{-3}	Test Conditions		Typical Specimen Photos
						Temperature/°C	Confining Pressure/MPa	
S-2	396.5	393.5	0.76%	190.3	2.08	150	10	
S-3	403.5	400.0	0.87%	191.7	2.11	150	20	
S-4	397.5	394.5	0.75%	192.4	2.07	150	30	
S-6	400.0	396.0	1.00%	192.8	2.07	100	30	
S-7	408.5	403.0	1.35%	192.8	2.12	180	30	
S-8	406.5	403.0	0.86%	192.4	2.11	250	30	

Table 2. Results of X-ray diffraction test and polarized microscope thin section analysis of sandstone specimens.

Mineral	Proportion (%)	Particle Size (mm)	Particle Structure	Photomicrograph of Sandstone
Quartz	53	0.2~0.5	Particle crushing (*Q*)	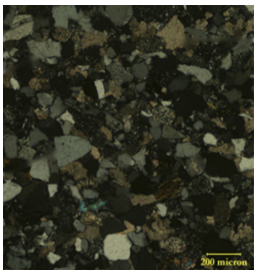
Calcite	16	0.5~1.0	Distinct twinkling (*Cal*)	
Plagioclase	14	0.4~0.6	Well-developed polysynthetic twins (*Pl*)	
Clay minerals	17	0.3~0.5	Flaky	

To ensure reliable test results, all specimens were cored from the same rock block to minimize heterogeneity. After cutting and grinding, specimens meeting the test requirements were selected. The specimens were heated in a muffle furnace at a heating rate of 10 °C/min, held at the target temperature for 2 h, and then cooled naturally. As shown in Table 1, the average mass loss rate of the specimens after heating was approximately 0.93%. Displacement control was adopted in the test. An initial preload of 1 kN was applied to fix the specimen. Confining pressure was then applied at a rate of 0.005 mm/s to the designated value. After the confining pressure stabilized, the axial load was reset to zero. Subsequently, with the confining pressure kept constant, axial load was applied at 0.005 mm/s until the specimen failed completely. Acoustic emission monitoring was performed throughout the test.

3. Test Results

3.1. Deformation and Failure Characteristics

Figure 3 shows the stress–strain curves and failure patterns of sandstone under different temperatures and confining pressures. Overall, the curves exhibit the following characteristics: At low stress levels, the curve bends upward as internal microcracks are closed (segment OA). Subsequently, the specimen enters an approximately linear elastic stage with a rapid increase in stress (segment AB). When the stress exceeds the crack initiation strength, internal cracks begin to propagate, the mechanical properties gradually weaken, and the curve deviates from linearity. Stress increases slowly until the volumet-

ric strain reaches its maximum and damage occurs (segment BC). After damage, cracks propagate rapidly, the curve shows an obvious deviation before the peak with noticeable fluctuations, and finally reaches the peak stress (segment CD). After the peak, the stress drops sharply with an indistinct residual stage, showing elastic–brittle behavior (segment DE). The overall process can be summarized as compaction—linear elasticity—crack initiation and propagation—damage—post-peak stress drop, which can be divided into five stages: compaction stage (OA), linear elastic stage (AB), stable crack propagation stage (BC), accelerated crack propagation stage (CD), and stress drop stage (DE). In terms of fracture characteristics, S-2 to S-4 exhibit predominantly vertical fractures with fracture angles ranging from 80° to 88°, while S-6 to S-8 are dominated by oblique fractures with fracture angles between 70° and 73°.

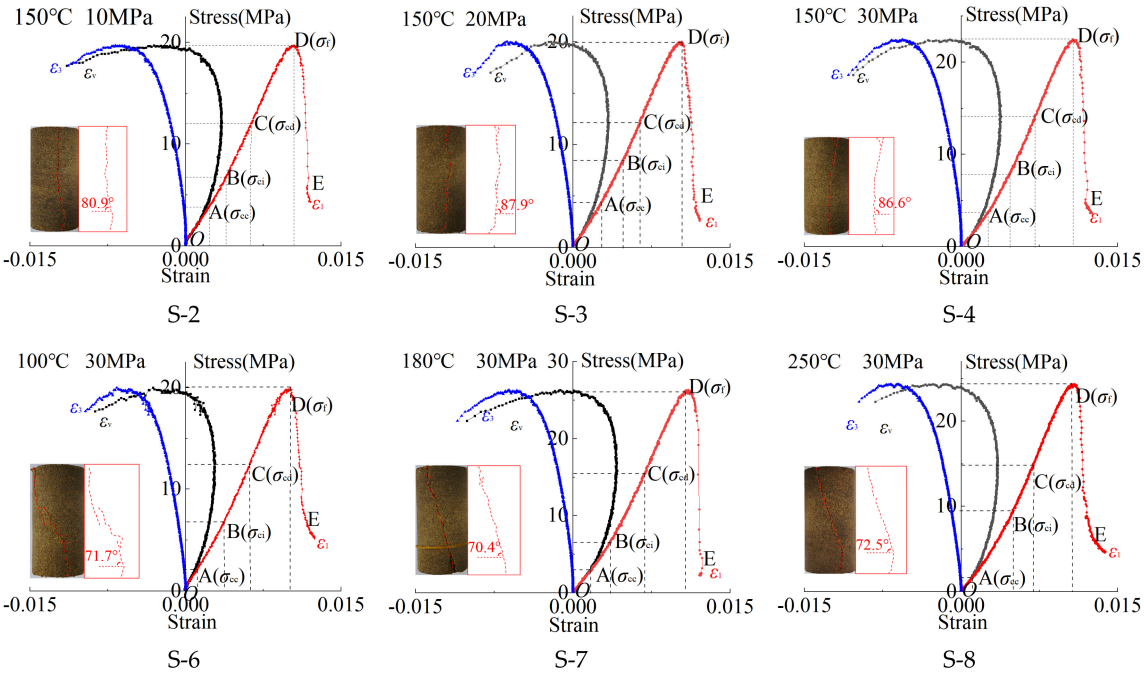

Figure 3. Stress–strain curves and failure patterns of sandstone under different temperatures and confining pressures.

3.2. Characteristics of Mechanical Parameters

Temperature and confining pressure affect not only the deformation and failure characteristics of sandstone, but also the evolution of its stress and strain mechanical parameters. Figures 4 and 5 below show the variation characteristics of damage strength, peak strength, elastic modulus and Poisson's ratio of sandstone under different confining pressures and temperatures. As shown in Figure 4a, at 150 °C with confining pressures ranging from 10 MPa to 30 MPa, the damage strength and peak strength of sandstone increase with increasing confining pressure. The peak strength ranges from 19.7 MPa to 22.46 MPa, and the damage strength ranges from 12.11 MPa to 14.1 MPa, with the ratio of damage strength to peak strength being approximately 0.6. As shown in Figure 4b, at 30 MPa and temperatures ranging from 100 °C to 250 °C, the damage strength and peak strength of sandstone first increase (100–200 °C) and then decrease (200–250 °C) with rising temperature, reaching their maximum values at 200 °C: 15.45 MPa and 26.29 MPa respectively.

According to Figure 5a, within the research range, the elastic modulus of sandstone ranges from 2.15 GPa to 2.53 GPa and increases with rising confining pressure, with an increase amplitude of 18%. The Poisson's ratio of sandstone ranges from 0.17 to 0.19. As shown in Figure 5b, the elastic modulus of sandstone first increases and then decreases with

rising temperature, reaching the maximum value of 2.95 GPa at 200 °C. The Poisson's ratio of sandstone first decreases and then increases with rising temperature, with a minimum value of 0.17.

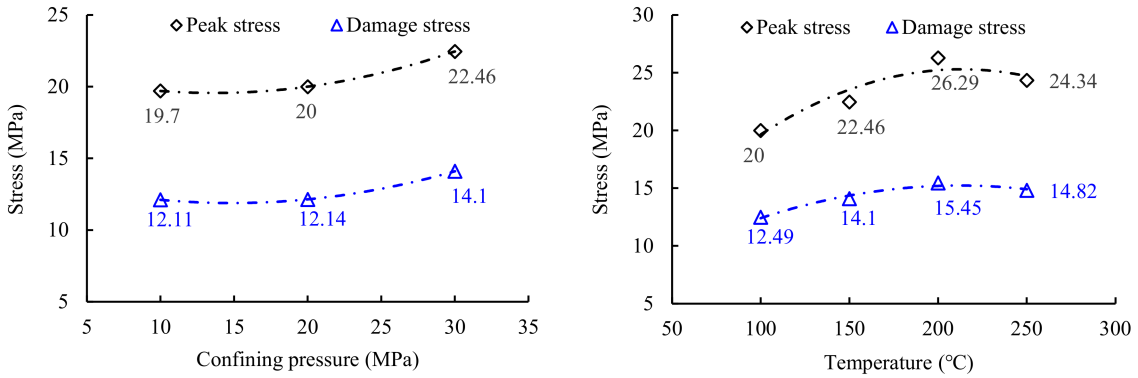

(**a**) (**b**)

Figure 4. Variation in stress characteristics of sandstone with confining pressure and temperature. (**a**) Variation in stress characteristics with confining pressure (150 °C). (**b**) Variation in stress characteristics with temperature (30 MPa).

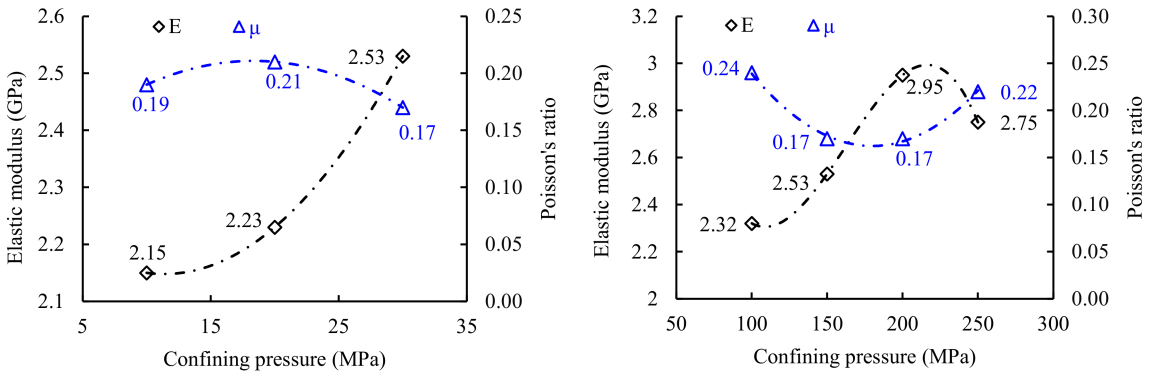

(**a**) (**b**)

Figure 5. Variation in deformation parameters of sandstone with confining pressure and temperature. (**a**) Variation in elastic modulus and Poisson's ratio with confining pressure (150 °C). (**b**) Variation in elastic modulus and Poisson's ratio with temperature (30 MPa).

3.3. Acoustic Emission Characteristics

Acoustic emission (AE) technology is an effective method for investigating crack propagation and damage evolution in brittle materials such as rock, and can well characterize the activity of microcracking events during crack evolution in rock (Eberhardt et al., 1998) [13]. The crack initiation stress σ_{ci} can be determined by the onset of significant AE activity, and the crack damage stress σ_{cd} by increasing AE bursts (Eberhardt et al., 1998) [13]. In this study, the AE method was adopted to obtain σ_{ci}, and the volumetric strain method was used to determine σ_{cd}. On this basis, the AE characteristics at different stress stages were analyzed. Figure 6 shows the time-dependent curves of stress and AE ring count for hot dry sandstone under thermal–mechanical coupling conditions. According to the different states of rock crack evolution, the stress–strain curve can be divided into stages with distinct mechanical significance, and the stress at each stage is defined as the characteristic stress. Based on these characteristic stress points, the acoustic emission signal characteristics during each evolutionary stage of the rock were analyzed. At the initial stage, the natural microcracks and pores inside the hot dry sandstone gradually close under external load, while no new microcracks are generated yet. Therefore, the acoustic emission activity is

relatively weak, and the ring count remains at a low level. When the axial stress reaches the crack initiation stress (σ_{ci}), the rock enters the stable crack propagation stage. In this stage, microcracks initiate randomly without obvious interaction or coalescence, the acoustic emission activity gradually increases, and the cumulative ring count grows steadily. As the axial stress continues to rise, the nucleation rate of internal microcracks accelerates, and they gradually interconnect. When the axial stress reaches the damage stress (σ_{cd}), the specimen enters the unstable crack propagation stage. In this stage, microcracks propagate and coalesce rapidly, forming distinct local fracture zones, resulting in intense acoustic emission activity and a significant increase in ring count. When the stress reaches the peak strength of the rock, internal microcracks connect rapidly to form a macroscopic fracture surface, and the acoustic emission ring count reaches its maximum. In the post-peak stage, under continuous axial loading, the rock undergoes further shear dislocation along the macroscopic fracture surface. Due to the interlocking and friction between crack surfaces, the acoustic emission activity remains relatively strong, and the ring count maintains a high level. In addition, the cumulative ring count increases approximately linearly and slowly before the peak, but rises rapidly after the peak strength.

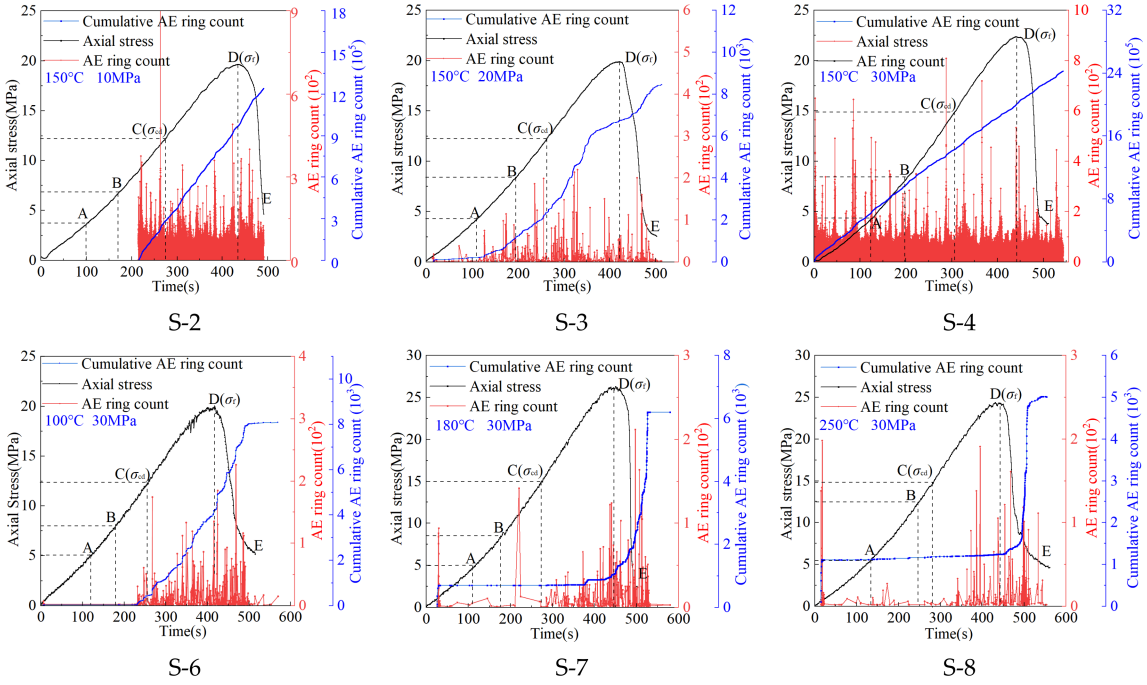

Figure 6. Relationship between stress and acoustic emission ringing count over time under different confining pressure and thermal conditions.

Figure 7 shows the time-dependent curves of stress and acoustic emission energy for hot dry sandstone under thermo-mechanical loading. At the initial loading stage, the original natural cracks and pores inside the sandstone gradually close under external load. Since no new microcracks initiate at this stage, acoustic emission signals are scarce, and the AE energy remains at a low level. When the axial stress exceeds the closure stress and further increases to the crack initiation stress, microcracks inside the rock begin to nucleate and propagate gradually. The initiation and propagation of cracks are accompanied by an increase in AE events, and the AE energy shows a slowly rising trend. As the axial stress increases from the crack initiation stress to the damage stress, a large number of microcracks propagate and gradually coalesce inside the sandstone. The interaction and connection of cracks release substantial elastic energy, causing a rapid increase in AE energy. When the axial stress reaches the peak strength of the rock, microcracks coalesce into macroscopic

cracks and form distinct fracture zones, accompanied by significant energy release, and the AE energy reaches its peak. Subsequently, under continuous axial loading, elastic energy is continuously released due to friction on the fracture surface, and the AE energy maintains a relatively high level in this stage. The cumulative AE energy varies with time as follows: it increases slowly and linearly before the peak strength, but rises rapidly after the peak strength.

AE can clearly capture the whole process of rock samples from micro-fracture initiation to macroscopic bursting failure, which presents outstanding advantages in identifying the precursor characteristics of rockbursts. Most existing studies establish a multi-parameter AE precursor index system using parameters such as b-value, energy release rate and ring-down count (Chen et al., 2026) [14]. A sharp rise in the cumulative AE energy curve of rock indicates that the engineering rock mass system approaches critical instability, and rockburst is imminent. For specimen S-7, AE events are sparse and relatively quiescent in the early stage, which facilitates internal energy accumulation. At the stage close to failure, AE events occur intensively with rapid energy release, leading to violent and sudden rock failure. Such failure characteristics are conducive to rockburst occurrence and can be regarded as effective rockburst precursors.

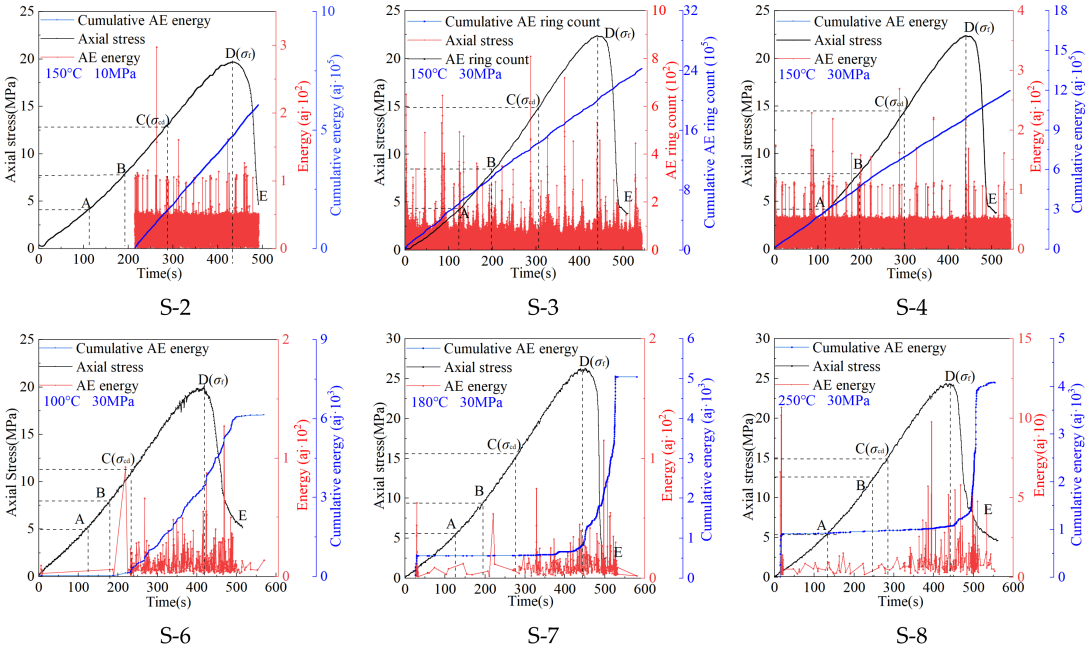

Figure 7. Relationship between stress and energy over time under different confining pressure and thermal conditions.

4. Energy Evolution Law

Energy dissipation occurs during the initiation, propagation, coalescence and slip of rock cracks in the failure process. Energy dissipation reflects the process of rock damage and degradation, and the essence of rock deformation and failure under loading is a process of energy dissipation. In this experiment, the sandstone specimens were first heated, then naturally cooled, and finally subjected to triaxial compression tests after cooling. Considering the deformation of rocks during triaxial compression, this process is assumed to be a closed system without heat exchange with the external environment. According to the first law of thermodynamics:

$$U = U_d + U_e + U_0 \quad (1)$$

where U is the total energy. U_d is dissipation energy. U_e is elastic strain energy. U_0 is the work done by the initial confining pressure on the sample at the beginning of the test.

The total energy U and the U_e elastic strain energy of rock can be calculated by the following formula:

$$U = \int \sigma_1 d\varepsilon_1 + 2\int \sigma_3 d\varepsilon_3 + U_0 \quad (2)$$

$$U_0 = \frac{3(1-2\mu)}{2E_0}\left(\sigma_3^0\right)^2 \quad (3)$$

$$U_e = \frac{1}{2E_u}\left[\sigma_1^2 + 2\sigma_3^2 - 2\mu\left(2\sigma_1\sigma_3 + \sigma_3^2\right)\right] \quad (4)$$

where E_0 and μ are the initial elastic modulus and initial Poisson's ratio of rock. E_u and μ are the unloading elastic modulus of rock and Poisson's ratio at unloading. σ_3^0 is the initial confining pressure value.

The statistical analysis of energy at the initial stage, damage stage, peak stage and residual stage of rock was carried out, and the results are shown in Figure 8. As shown in Figure 8, the elastic strain energy is greater than the dissipated energy at the initial and damage stages. However, the dissipated energy is larger than the elastic strain energy at the peak and residual stages. This indicates that before damage, the work done by external forces is mainly converted into elastic strain energy, whereas after damage, it is primarily transformed into dissipated energy. The total energy exhibits an increasing trend throughout the entire process, with a relatively large increment before the damage point and a smaller increment after damage. At the initial stage, all specimens possess a certain amount of dissipated energy, accounting for 0.05–18.80% of the total energy, which is mainly related to the inherent properties of the sandstone specimens. As mentioned previously, the strength of the sandstone specimens in this study is relatively low, with peak strength ranging from 19.7 MPa to 22.46 MPa under confining pressures of 10–30 MPa. Therefore, prior to axial loading, microcracks may have occurred in weaker zones inside the specimens, leading to a certain amount of energy consumption. Similarly, at the residual stage, all specimens retain a considerable amount of elastic strain energy, accounting for 10.93–42.95% of the total energy. Such a relatively high proportion is mainly attributed to the confining pressure. Even after failure, the specimen remains in a compressed state due to confining pressure, with a certain amount of elastic strain energy still stored inside. By comparing the ratio curves of elastic strain energy to total energy, it can be found that with the increase in stress and the progressive deterioration of the specimen, the ratio of elastic strain energy to total energy decreases continuously. In contrast, the ratio of dissipated energy to total energy increases gradually.

To further analyze the effects of confining pressure and temperature on the energy evolution law, the energy values at the damage point and peak point were selected for in-depth analysis, and the results are shown in Figure 9. As shown in Figure 9a, the total energy, elastic strain energy and dissipated energy exhibit the same variation trend with increasing confining pressure, characterized by first increasing and then decreasing. At 20 MPa, the total energy, elastic strain energy and dissipated energy all reach their maximum values at both the damage point and the peak point. The maximum total energy at damage is 0.43 MJ/m^3, and that at the peak is 0.56 MJ/m^3. The dispersion of energy data is the largest at 20 MPa and the damage point. At the peak point, the values of dissipated energy and elastic strain energy are close to each other. As shown in Figure 9b, all energy components show similar variation trends with temperature. Energy decreases significantly in the range of 100–150 °C. In the range of 150–180 °C, energy obviously increases, but the increment is smaller than the previous decrement. Energy decreases slightly in the range of 180–250 °C. All energy components reach their minimum values at 150 °C. For

example, the total energy at damage is 0.24 MJ/m^3, and that at the peak is 0.37 MJ/m^3. Comparative analysis of energy evolution with confining pressure and temperature shows that the dispersion of elastic strain energy and dissipated energy is relatively small under different temperatures, but larger under different confining pressures. Meanwhile, at the peak point, elastic strain energy and dissipated energy are close in magnitude, while the difference is more significant at the damage point. This indicates that confining pressure and temperature exert different influences on the energy evolution of the specimens at different stages, and the energy response may be more sensitive at the damage stage.

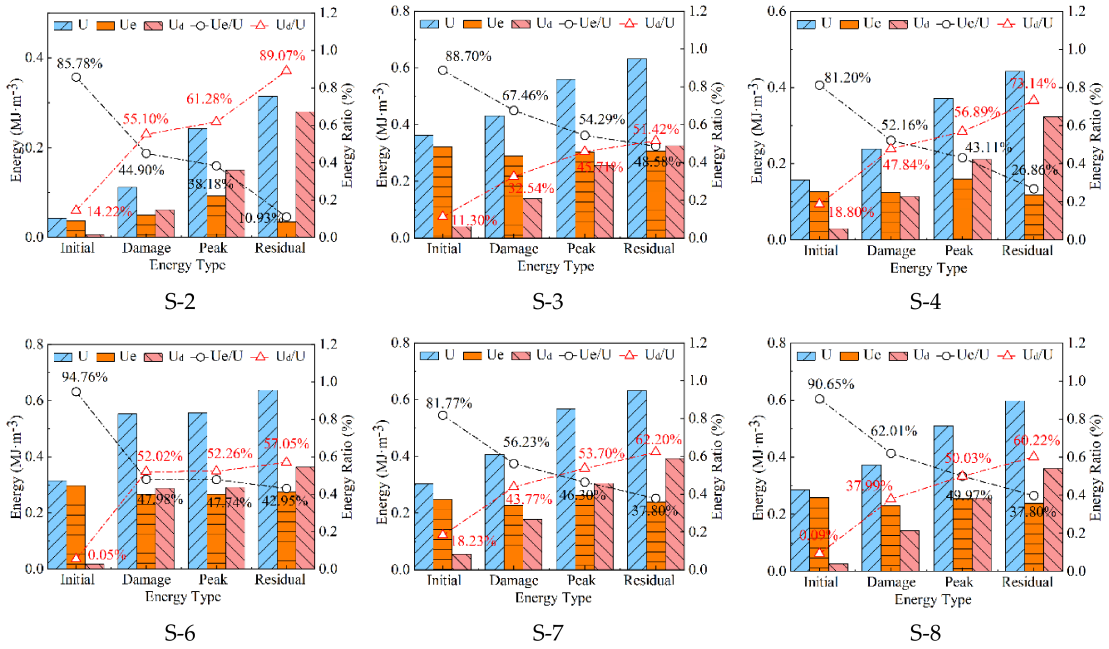

Figure 8. Statistical analysis of energy at each stage for sandstone specimens.

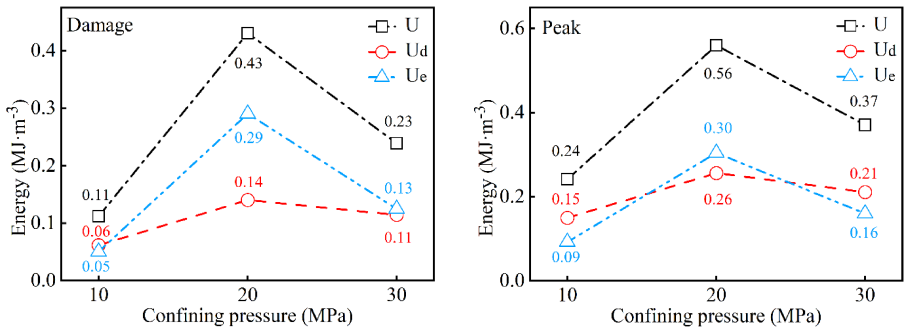

(**a**) Variation in energy with confining pressure

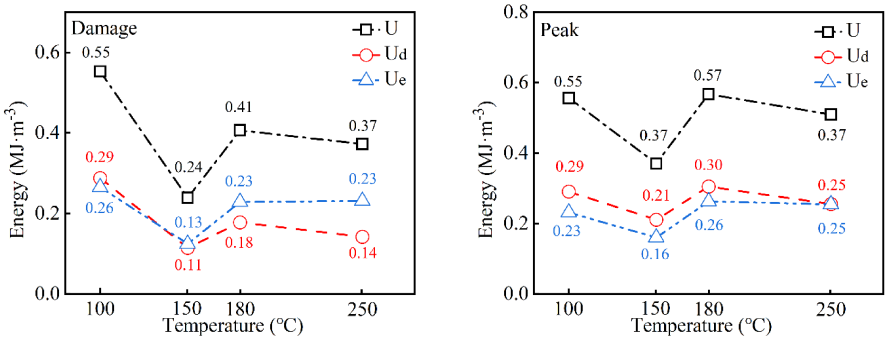

(**b**) Variation in energy with temperature

Figure 9. Variation in energy with confining pressure and temperature.

5. Discussion

5.1. Sensitivity Analysis

The influence of temperature and confining pressure on the mechanical properties of sandstone is analyzed by means of the sensitivity coefficient. The formula for calculating the sensitivity coefficient is as follows:

$$S = \frac{\Delta A}{A} \div \frac{\Delta B}{B} \tag{5}$$

where S represents the sensitivity coefficient, ΔA and A denote the variation and original value of the dependent variable, respectively, and ΔB and B denote the variation and original value of the independent variable, respectively.

As shown in Figure 10a, significant differences in the mechanical properties of rock are observed when the confining pressure increases from 10 MPa to 20 MPa and 30 MPa. The sensitivity of peak strength to confining pressure increases remarkably with rising confining pressure. When the confining pressure increases from 10 MPa to 20 MPa, the sensitivity coefficient rises significantly from 0.015 to 0.070, representing a 4.7-fold increase. This indicates that within a relatively low confining pressure range, the sandstone strength responds slowly to the increase in confining pressure. However, once the confining pressure exceeds a certain critical value (10 MPa), the sensitivity of rock strength to confining pressure increases sharply, and the strengthening effect of confining pressure becomes prominent. In contrast, the sensitivity of volumetric peak strain to confining pressure is relatively stable. When the confining pressure increases from 10 MPa to 20 MPa and 30 MPa, the sensitivity coefficients are 0.311 and 0.322 respectively, showing only a 3.5% increase. This result suggests that the volumetric deformation of sandstone responds slowly to changes in confining pressure, and the deformation resistance of the rock does not change significantly during the increase in confining pressure but tends to be stable.

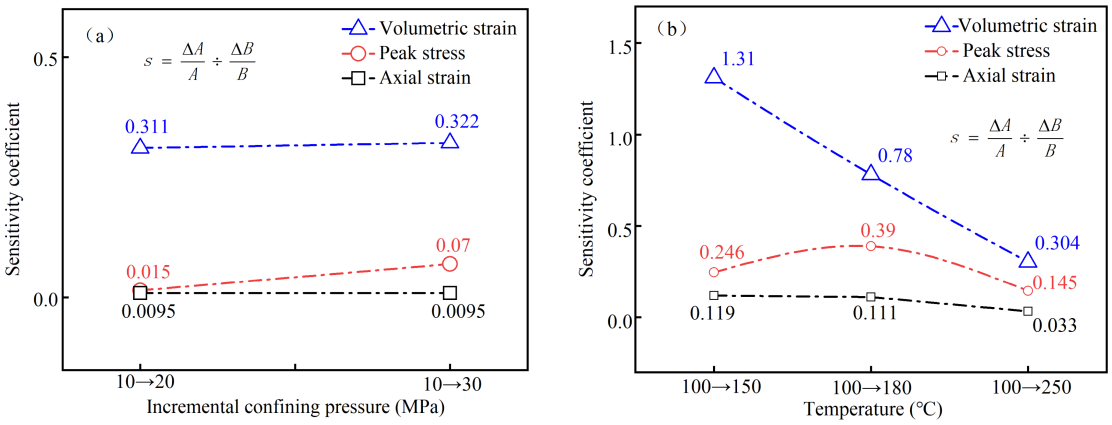

Figure 10. Sensitivity analysis diagram. (**a**) Sensitivity to confining pressure; (**b**) Sensitivity to temperature.

As shown in Figure 10b, when the temperature increases from 100 °C to 150 °C, 180 °C and 250 °C respectively, various mechanical parameters exhibit different degrees of sensitivity to temperature change. The sensitivity of peak strength to temperature shows a trend of increasing first and then decreasing. When the temperature rises from 100 °C to 180 °C, the sensitivity coefficient increases from 0.246 to 0.390, indicating that the response of sandstone peak strength to temperature change is significantly enhanced within this temperature range. However, when the temperature further rises to 250 °C, the sensitivity coefficient decreases to 0.145, suggesting that beyond a certain temperature threshold, the sensitivity of peak strength to temperature decreases significantly, and the weakening effect of temperature on sandstone strength tends to moderate. The sensitivity

of axial peak strain to temperature shows an overall gradual decreasing trend. When the temperature rises to 150 °C and 180 °C, the sensitivity coefficients of axial peak strain are 0.119 and 0.111 respectively, with no obvious change. After further increasing to 250 °C, the sensitivity coefficient drops significantly to 0.033, indicating that the sensitivity of axial deformation to temperature rise is greatly weakened at high temperatures, and the ductile deformation response of sandstone tends to be stable. The sensitivity of volumetric peak strain decreases significantly with increasing temperature. The sensitivity coefficient gradually decreases from 1.310 (100–150 °C) to 0.780 (150–180 °C) and 0.304 (180–250 °C), indicating that with continuous temperature rise, the sensitivity of sandstone volumetric deformation to temperature change is significantly weakened. This reflects that the thermal damage of internal pores and microcracks tends to stabilize gradually at high temperatures, and the volumetric response of the rock structure is gradually reduced.

In summary, confining pressure exhibits a significant differential effect on the peak strength and deformability of sandstone, among which the sensitivity of rock strength to confining pressure variation is much higher than that of volumetric deformation. It can be inferred that the strength enhancement effect of sandstone under confining pressure is significantly greater than the improvement of its deformation resistance, and the change in confining pressure has a more prominent influence on sandstone strength. This phenomenon reveals the decisive role of internal crack closure and structural densification of sandstone under confining pressure in determining rock strength. Obvious differences exist in the sensitivity of sandstone peak strength and strain to temperature variation. The sensitivity of peak strength shows a trend of first increasing and then decreasing, whereas the sensitivity of axial and volumetric strains gradually decreases with rising temperature. This characteristic reflects that there exists an obvious thermal damage threshold for rock mechanical properties within a specific temperature range.

5.2. Analysis of the Particle Effect of Sandstone

The size of mineral particles and the distribution and arrangement of cementation between mineral particles have an important influence on the rock failure mechanism. Sandstone is mainly cemented by sand grains, and sand grains with different shapes and sizes exert different effects on its fracture behavior. Regarding the particle effect analysis [15–18], Wang et al. (2018) suggested that under the same loading condition, sandstone with a larger particle size is more prone to failure with more intense fracture behavior [15]. Wang et al. (2023) pointed out that increasing heterogeneity of mineral elastic modulus leads to unsynchronized damage of adjacent mineral particles, enhancing the nonlinear characteristics of rock deformation [16]. The tangential modulus and compressive strength decrease linearly, accompanied by reduced crack initiation stress and damage stress. The macroscopic failure mode transforms from shear failure to splitting failure. However, under the same heterogeneity of mineral elastic modulus, different spatial distributions of mineral particles result in excessive elastic modulus differences between adjacent grains. During compression, incompatible deformation between adjacent particles forms "weak contact surfaces" in mechanical parameters, promoting the initiation, propagation and coalescence of mesoscopic cracks [17].

Sandstone is composed of mineral particles, cement and pores. As shown in Figure 11, irregular particle arrangement structures can be observed inside sandstone specimens. Particles are bonded by cement, accompanied by natural intergranular pores and initial microdefects. Such microscopic inhomogeneities act as intrinsic factors governing the mechanical behavior of sandstone and serve as preferential sites for crack initiation. The fracture process of sandstone can be divided into three progressive stages: crack initiation, crack propagation and macroscopic failure formation (Figure 11), which reflects the particle

scale effect featuring gradual failure evolution from intergranular damage to intragranular fracture (Table 3).

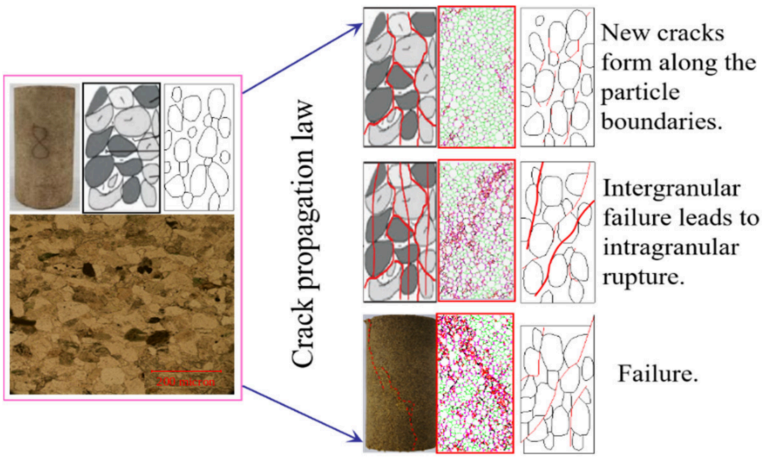

Figure 11. Schematic diagram of sandstone failure mechanism considering particle effect (modified 2024 [18]).

Table 3. Correspondence between macro and micro-fracture characteristics of sandstone.

Mechanical Stage	Microscopic	Macroscopic
Compaction stage (OA)	Initial pore closure	Concave-up stress–strain curve with nonlinear deformation
Linear elastic stage (AB)	Elastic compression of grains and load bearing by cement	Linear stress–strain relationship with uniform volumetric contraction
Stable crack propagation stage (BC)	Initiation and stable propagation of intergranular cracks	Deviated linear stress–strain curve and initial dilatancy
Accelerated crack propagation stage (CD)	Coalescence of intragranular and transgranular cracks	Stress reaches peak strength, and volumetric strain shifts from compression to dilation
Stress drop stage (DE)	Grain slippage	Stress drop, residual strength dominated by intergranular friction

Stage 1: Due to the mechanical property discrepancy between particles and cement, grain interfaces become relatively weak regions. When stress exceeds cementation strength, new cracks preferentially initiate and propagate along grain boundaries. A large number of intergranular cracks form in this stage, with crack networks distributed along grain contours, which macroscopically corresponds to the late period of rock compaction and linear elastic stages.

Stage 2: With increasing stress, cracks propagating along grain boundaries gradually coalesce to form localized deformation bands. As the intergranular crack network develops, the stress transfer path reconstructs. Grains in partially high-stress concentration zones bear stress exceeding their inherent strength, driving cracks to extend from grain boundaries into grain interiors, namely the transformation from intergranular failure to transgranular fracture. This stage acts as a critical transition from stable deformation to unstable failure. Macroscopically, the stress–strain curve deviates from linearity, accompanied by prominent nonlinear characteristics and volumetric dilatancy.

Stage 3: The full coalescence of intragranular and transgranular cracks eventually forms macroscopic fracture surfaces. The interlocking effect between grains is substantially weakened, leading to a sharp decline in bearing capacity, which corresponds to the stress drop stage macroscopically.

Based on existing studies, it is concluded that at the initial stage, primary cracks and microvoids in sandstone close first. During the crack incubation stage, cracks preferentially initiate along grain boundaries. During the unstable crack propagation stage, incompati-

ble deformation between adjacent particles causes some cracks to penetrate crystals and form transgranular cracks [17,18]. With the connection and convergence of cracks, final penetration leads to specimen failure (Figure 11).

5.3. Thermal Effect

Some scholars have proposed two explanations for the enhanced rock properties after heat treatment (Figure 12). On the one hand, under relatively low temperatures, thermal expansion of internal mineral grains gradually closes primary fractures within rocks (Yu et al., 2015) [19]. The reduced pore volume and improved compactness optimize the contact state between mineral particles (Yin et al., 2012) [20]. On the other hand, temperature rise evaporates adsorbed and interlayer water inside rocks, weakening the lubrication effect for grain sliding and enhancing interfacial friction characteristics.

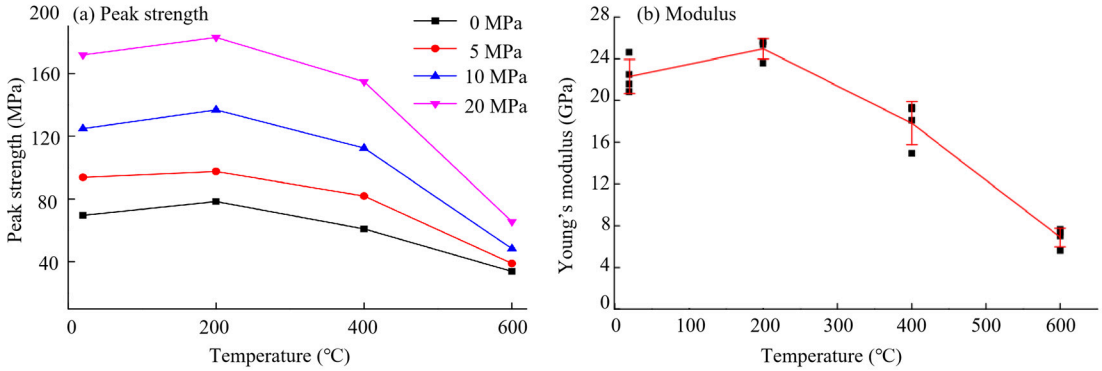

Figure 12. Mechanical parameters of sandstone under different confining pressures after heat treatment (Yu et al., 2015) [19].

The temperature enhancement effect of sandstone is analyzed from the perspectives of thermal strain and negative strain energy. As shown in Figure 13, thermal strain generally rises with increasing temperature. It increases rapidly within 100–180 °C and tends to stabilize at 180–250 °C, indicating thermal expansion of quartz, calcite, plagioclase, clay minerals and other constituents during heating. When thermal stress induced by temperature rise does not exceed intergranular bonding strength, sandstone properties will not degrade. Instead, thermal expansion compresses internal pores and elevates the effective contact degree between mineral particles. Continuous accumulation of negative strain energy can be observed in Figure 14. Such accumulated negative strain energy offsets partial external work under axial loading, thereby boosting bearing capacity and optimizing mechanical properties to a certain extent.

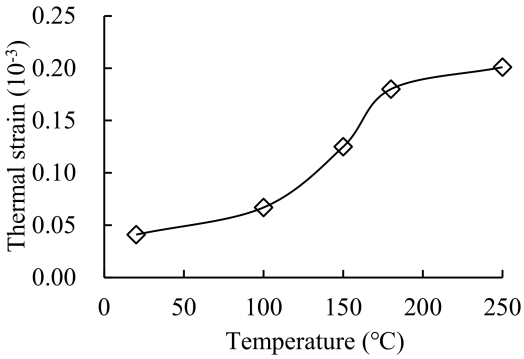

Figure 13. Thermal-strain curve under different temperatures.

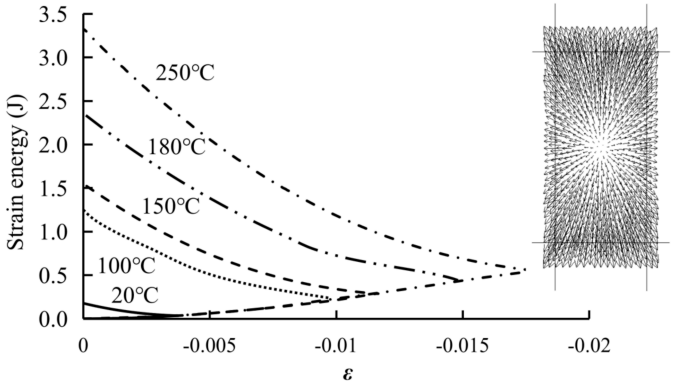

Figure 14. Strain-energy curve of the heating process.

5.4. Statistical Damage Constitutive Model

Sandstone contains numerous randomly distributed defects such as pores, microcracks and joints, and thus can be regarded as a porous medium. Affected by pores and other defects, the strength of rock mesoscopic elements presents random variations. The two-parameter Weibull distribution function exhibits superior descriptive capability and can well characterize the variation characteristics of rock element strength. Accordingly, the Weibull distribution is adopted to establish the constitutive model from the perspective of statistical damage. According to damage mechanics, the process of a material from the initiation of damage to failure is continuous. Therefore, it is assumed that the material is composed of isotropic elements that obey the generalized Hooke's law, and the strength of each element follows the Weibull distribution, whose probability density function P(F) is given by:

Density function:

$$F(k) = 1 - \exp\left[-\left(\left(\frac{k}{F}\right)^{m}\right)\right] \tag{6}$$

where m and f are the shape parameter and scale parameter of the Weibull function, which correspond to the homogeneity and peak strength of concrete, respectively. k represents the strength of rock mesoscopic elements ($k = \alpha_0 I_1 + \sqrt{J_2}$).

Under the combined action of temperature and pressure, the meso-elements continue to fracture, resulting in rock damage. Assuming that the number of failed meso-elements is N_f and the total number of meso-elements is N, the statistical damage variable D is defined as:

$$D = N_f/N \tag{7}$$

At the stress level of $f(\sigma)$, the number of damaged rock elements N_f is:

$$N_f = \int_0^{f(\sigma)} Nf(\sigma)d\sigma = N\int_0^{f(\sigma)} f(\sigma)d\sigma \tag{8}$$

Substitute Equation (8) into Equation (7), and the damage variable D is:

$$D = N_f/N = \left(N\int_0^{f(\sigma)} f(\sigma)d\sigma\right)/N = \int_0^{f(\sigma)} f(\sigma)d\sigma = 1 - \exp\left\{-\left[\frac{f(\sigma)}{F}\right]^{m}\right\} \tag{9}$$

The Drucker–Prager criterion is introduced as the failure criterion, namely:

$$f(\sigma) - k = 0 \tag{10}$$

Substituting Equation (10) into Equation (9), and considering $\sigma_2 = \sigma_3$ in the triaxial test, the constitutive model is expressed as follows:

$$\sigma_1 = E_T \varepsilon_1 \exp\left[-\left(\left(\frac{\alpha_0 I_1 + \sqrt{J_2}}{F}\right)^m\right)\right] + 2\mu\sigma_3 \tag{11}$$

Substitute the peak point (ε_c, σ_c) into Equation (11), yielding:

$$\sigma_c = E_T \varepsilon_c \exp\left[-\left(\left(\frac{\alpha_0 I_1 + \sqrt{J_2}}{F}\right)^m\right)\right] + 2\mu\sigma_3 \tag{12}$$

By partially differentiating Equation (12), the first derivative at the peak point is zero. Substitution yields:

$$\left.\frac{\partial\sigma_1}{\partial\varepsilon_1}\right|_{\varepsilon=\varepsilon_c} = E_T \exp\left[-\left(\left(\frac{\alpha_0 I_1 + \sqrt{J_2}}{F}\right)^m\right)\right] + E_T\varepsilon_c \exp\left[-\left(\left(\frac{\alpha_0 I_1 + \sqrt{J_2}}{F}\right)^m\right)\right] \times \left\{-m\left[\left(\frac{\alpha_0 I_1 + \sqrt{J_2}}{F}\right)^{m-1}\right]\right\} \times \left[\frac{\frac{\alpha_0(\sigma_c + 2\sigma_3)E_T}{\sigma_c - 2\mu\sigma_3} + \frac{(\sigma_c - \sigma_3)E_T}{\sqrt{3}(\sigma_c - 2\mu\sigma_3)}}{F}\right] = 0 \tag{13}$$

Rearranging Equations (12) and (13) gives:

$$\begin{cases} m = \dfrac{1}{ln\dfrac{E_T\varepsilon_c}{\sigma_c - 2\mu\sigma_3}} \\ F = \dfrac{\left[\alpha_0(\sigma_c + 2\sigma_3) + \dfrac{\sqrt{3}}{3}(\sigma_c - \sigma_3)\right]\dfrac{E_T\varepsilon_c}{\sigma_c - 2\mu\sigma_3}}{\left(ln\dfrac{E_T\varepsilon_c}{\sigma_c - 2\mu\sigma_3}\right)^{\frac{1}{m}}} \end{cases} \tag{14}$$

After parameter solving (Table 4) (Gao et al., 2018; Zhang et al., 2021; Gao et al., 2024) [21–23], the experimental parameters are substituted into the constitutive equation to obtain the theoretical constitutive curve. The rationality of the constitutive model is verified by comparison with the experimental curves. Figure 15 shows the comparison between the experimental and theoretical results of the stress–strain curves of sandstone. As shown in Figure 15, when the stress–strain curve of the specimen develops from the damage stage to the post-peak stage, the stress growth rate gradually slows down, and the stress drops rapidly after the peak, showing obvious brittle failure characteristics. The theoretical curve and the experimental curve basically coincide with good matching characteristics. It can be seen that the constitutive model established based on statistical damage can accurately describe its damage evolution law and deformation characteristics, and is more consistent with the actual failure law of rock.

Table 4. The values of constitutive model parameters for each sample.

NO.	σ_c/MPa	ε_c	*E*/GPa	μ	*F*/MPa	*m*
SY-2	19.7	0.010488	2.15	0.19	25.8	0.5
SY-3	22.5	0.010730	2.51	0.17	45.1	3.1
SY-4	20.0	0.010392	2.23	0.20	23.9	1.2
SY-6	20.0	0.010130	2.31	0.24	22.2	1.0
SY-7	26.3	0.011008	2.89	0.17	91.2	4.7
SY-8	24.3	0.010619	2.83	0.21	38.0	1.5

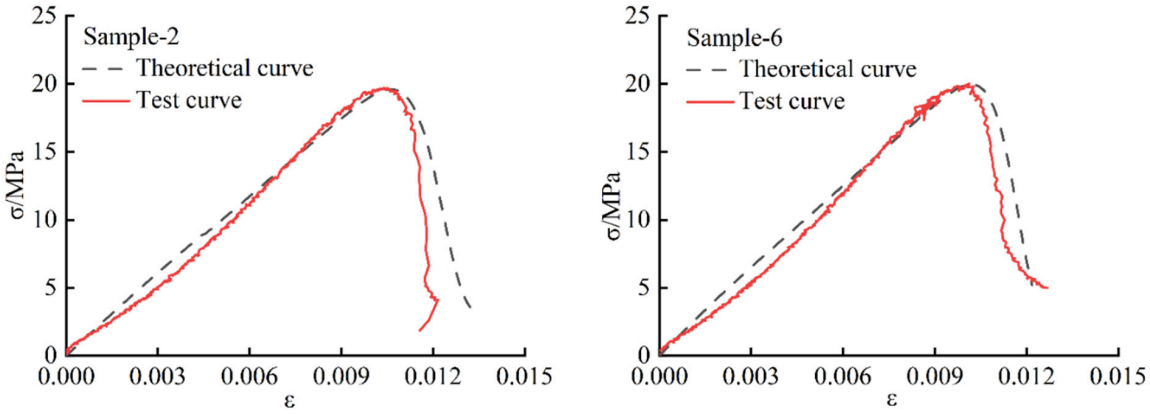

Figure 15. Experimental and theoretical stress–strain curves.

5.5. Implications for Rockburst Prevention and Control

Many adverse geological problems encountered in tunnel engineering in sandstone strata are closely related to the inherent brittleness of sandstone. As a typical brittle material, sandstone exhibits a Type II failure characteristic in its stress–strain curve (Figure 16). Rockburst is essentially a catastrophic phenomenon induced by energy evolution during the crack initiation and brittle fracture process of the tunnel surrounding rock. In recent years, with the implementation of a series of major engineering projects in Western China, a large number of deep-buried long and large tunnels have emerged. However, Western China is located in the orogenic belt formed by the compression of the Indian Plate and the Eurasian Plate. The mutual collision and convergence of crustal plates have resulted in a complex continental crustal convergence—a chimeric tectonic setting. In particular, since the Quaternary period, the Y-shaped tectonic belt has been reactivated under the intracontinental collision and compression between the Qinghai–Tibet Plate and the Yangtze Plate, forming a complex geological environment characterized by the coupling of high in situ stress and high geotemperature. Such a complicated geological environment inevitably exerts a significant impact on engineering construction in this region. For example, more than 200 rockbursts of varying intensities occurred successively during the construction of the Erlangshan Tunnel on National Highway 318 (Figure 17), distributed across 15 sections with a total length of 1776 m. The lithology is dominated by hard and brittle sandstone, sandy mudstone, and quartz sandstone [24]. Meanwhile, among the 13 engineering geological rock groups along the under-construction CZ Railway in Western China, as many as seven contain sandstone (Table 5), indicating its wide distribution and high proportion. At present, investigations into the energy evolution characteristics and fracture mechanism of sandstone under thermo-mechanical coupling can provide effective technical support for the prevention and control of geological hazards such as rockbursts in sandstone strata along the CZ Railway.

The study reveals that the increase in confining pressure can significantly enhance the strength properties of sandstone, and temperature rise within a certain range (100–180 °C) can also improve its strength. This indicates that a high-temperature and high-stress environment may be conducive to the occurrence of rockbursts. In the preliminary engineering demonstration stage, sections prone to rockbursts under high ground temperature and high in situ stress should be avoided as far as possible. Meanwhile, during the construction of deeply buried tunnels with high ground temperature, such as the CZ Railway tunnels, it is necessary to reasonably control the stress concentration degree and construction temperature of surrounding rocks. This measure can mitigate thermal shock induced by temperature difference and instability caused by stress concentration, thereby reducing sudden rockburst disasters and corresponding engineering risks.

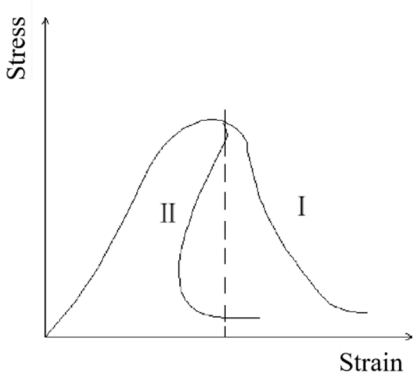

Figure 16. Failure types of rock under uniaxial compression.

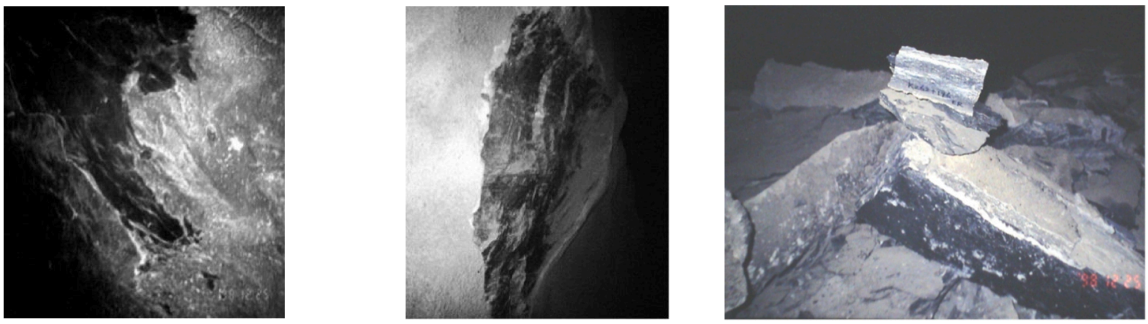

(**a**) Conchoidal rockburst fracture surface (**b**) Fresh surface of rockburst (**c**) Platy rockburst rock fragments

Figure 17. Typical failure signs of rockburst in the Erlangshan Tunnel on National Highway 318 [24].

Table 5. List of engineering geological rock masses along and adjacent to the CZ Railway.

No.	Engineering Geological Rock Mass	Area (km^2)	Proportion (%)
1	Hard, thick-bedded sandstone rock mass	17,835.7	1.6
2	Medium-hard to hard medium-thick bedded sandstone intercalated with conglomerate, mudstone and slate rock mass	114,246.3	10.3
3	Medium-thick bedded sandstone and mudstone with alternating soft and hard layers, intercalated with limestone and argillaceous limestone, as well as their interbedded rock mass	203,712.2	18.4
4	Weak to medium-hard thin to medium-thick bedded interbedded sandstone, mudstone, conglomerate and argillaceous rock mass	67,185.8	6.1
5	Weak thin-bedded mudstone and shale rock mass	70,239.2	6.3
6	Hard, medium-thick bedded limestone and dolomite rock mass	35,793.8	3.2
7	Medium-hard thin- to medium-thick bedded limestone and argillaceous limestone rock mass	33,039.3	3.0
8	Medium-hard to hard medium-thick bedded limestone and dolomite rock mass intercalated with sandstone, mudstone, phyllite and slate	60,239.2	5.4
9	Medium-hard to hard thin- to medium-thick bedded interbedded rock mass of slate, phyllite and metamorphic sandstone	73,724.0	6.7
10	Weak to medium-hard thin- to medium-thick bedded phyllite and schist intercalated with limestone, sandstone and volcanic rock mass	140,566.2	12.7
11	Massive basalt-dominated hard rock mass	20,639.4	1.9
12	Hard massive rock mass of granite, andesite and diorite	170,171.5	15.4
13	Soft, loose structure rock mass	100,085.6	9.0

6. Conclusions

In this paper, triaxial compression tests and acoustic emission monitoring were carried out to explore the deformation and failure characteristics, mechanical parameters, acoustic emission features, and energy evolution laws of sandstone under confining pressures of 10–30 MPa and temperatures of 100–250 °C. The sensitivities to confining pressure and temperature, as well as the particle effect, were discussed. A statistical damage constitutive model was established, and implications for rockburst prevention and control in tunnel engineering were revealed. Considering that each parameter combination was only tested once without repeated trials and statistical analysis, the preliminary conclusions are presented as follows:

(1) The deformation of sandstone generally exhibits the characteristics of compaction, linear elasticity, crack initiation and propagation, stable crack propagation stage, accelerated crack propagation stage, and stress drop stage. The fracture angle ranges from 60° to 90°, representing typical brittle failure. The peak strength and damage strength increase with the rise in confining pressure and temperature. The elastic modulus increases with increasing confining pressure.

(2) It can be inferred from the sandstone test results that the damage point of the rock may serve as the critical point for energy conversion and acoustic emission (AE) activities. After damage, the work done by an external force is mainly converted into dissipated energy. Acoustic emission activities rise markedly at the damage stress and reach the maximum at peak strength. Both cumulative AE ring-down counts and cumulative energy increase slowly before the peak stress and grow rapidly after the peak stress. The discreteness of elastic strain energy and dissipated energy is relatively slight under different temperature conditions, while it becomes more prominent under various confining pressures.

(3) The fracture mechanism considering the particle effect of sandstone is described as follows: cracks preferentially initiate along grain boundaries, and incompatible deformation between particles promotes the formation of transgranular cracks. The connection and coalescence of these cracks eventually lead to specimen failure. A thermal–mechanical statistical damage constitutive model for sandstone was established. The theoretical curves agree well with the test curves, which effectively verifies the rationality of the model. The model can accurately describe the damage evolution and deformation characteristics and is more consistent with the actual rock failure mechanism.

(4) Within a certain range, the elevation of temperature and confining pressure can enhance the bearing capacity of sandstone, indicating that a high-temperature and high-stress environment may be conducive to the occurrence of rockbursts. In engineering practice, sections prone to rockbursts induced by high ground temperature and high in situ stress should be avoided as far as possible. During construction, reasonable regulation of surrounding rock stress concentration and temperature can effectively mitigate thermal shock caused by temperature difference and instability induced by stress concentration, thereby reducing sudden rockburst disasters and engineering risks.

It is further pointed out that rockburst occurrence is affected by numerous factors, including rock lithology, in situ stress, geological structures, groundwater, seismic activity and geotemperature. Combined with the geological characteristics of high ground temperature up to 150 °C and burial depth ranging from 1000 m to 3000 m in Kangding, Sichuan Province, this study conducted sandstone tests under temperatures of 100–250 °C and confining pressures of 10–30 MPa. The temperature effect was preliminarily analyzed from the perspectives of rock lithology, confining pressure and temperature, which serves as a pilot

study. The research findings can provide references and guidance for subsequent relevant investigations. Nevertheless, only one specimen was tested under each temperature and confining pressure condition, so the statistical regularity of the obtained results remains to be verified. Accordingly, further systematic research will be carried out by the research group to clarify the influences of medium-low temperature (room temperature to 250 °C) and confining pressure on the mechanical properties, fracture mechanisms and rockburst propensity of sandstone, so as to draw universally applicable conclusions.

Author Contributions: M.G.: Conceptualization, data analysis and original draft. M.H. and R.C.: Tests and literature search. S.Q. and F.Z.: Data analysis and literature search. Y.Z. and T.L.: Conceptualization, review and editing. All authors have read and agreed to the published version of the manuscript.

Funding: This work was funded by the National Natural Science Foundation of China (42130719), Humanities and Social Sciences Research Project of Ministry of Education (23YJCZH051), the Opening fund of State Key Laboratory of Geohazard Prevention and Geoenvironment Protection (Chengdu University of Technology) (SKLGP2025K023), and the Opening Foundation of Key Laboratory of Landslide Risk Early-warning and Control, Ministry of Emergency Management (Chengdu University of Technology) (KLLREC2022K003), for which the authors are grateful.

Institutional Review Board Statement: Not applicable.

Informed Consent Statement: Not applicable.

Data Availability Statement: The data that support the findings of this study are available from the corresponding author upon reasonable request.

Conflicts of Interest: The authors declare no conflicts of interest.

References

1. Gao, M.B.; Li, T.B.; Ji, S.X.; Bai, S.M.; Zhang, Y.; He, Z.H.; Zhang, L. A prediction model for high-geothermal rockburst intensity using a genetic projection pursuit algorithm. *J. Rock Mech. Geotech. Eng.* **2025**, *17*, 7612–7627. [CrossRef]
2. Li, J.Y.; Liu, D.Q.; He, M.C.; Guo, Y.P. Experimental Investigation on Rockburst Energy Characteristics of True Triaxial Unloading in Sandstone Under High Stress. *Rock Mech. Rock Eng.* **2024**, *57*, 6031–6046. [CrossRef]
3. Mazaira, A.; Konicek, P. Intense Rockburst Impacts in Deep Underground Construction and Their Prevention1. *Can. Geotech. J.* **2015**, *52*, 1426–1439. [CrossRef]
4. Sun, X.M.; Ren, C.; Liu, D.Q.; He, M.C.; Yang, J.K.; Li, Z.H.; Zhu, J.J.; Yuan, J.C.; Qi, Z.M. Mechanism Analysis and Type Determination of The Rockburst of the Gaoloushan Tunnel Based on A Study of Rockburst Fragments. *Chin. J. Eng.* **2023**, *45*, 337–348.
5. Tian, H.; Kempka, T.; Yu, S.; Ziegler, M. Mechanical Properties of Sandstones Exposed to High Temperature. *Rock Mech. Rock Eng.* **2016**, *49*, 321–327. [CrossRef]
6. Gao, Z.L.; Liu, Z.B.; Tian, F.; Shen, W.Q. Strength, energy evolution and cracking process of sandstone under high-temperature and high-pressure coupled true triaxial compression. *Geomech. Geophys. Geo-Energy Geo-Resour.* **2022**, *8*, 176. [CrossRef]
7. Liu, L.Y.; Jin, J.; Liu, J.D.; Cheng, W.; Zhao, M.H.; Luo, S.W.; Luo, Y.; Wang, T. Mechanical properties of sandstone under in-situ high-temperature and confinement conditions. *Int. J. Miner. Metall. Mater.* **2025**, *32*, 778–787. [CrossRef]
8. Jin, J.; Liu, J.D.; Chen, W.X.; Li, G.P.; Cheng, W.; Zhang, X.W.; Luo, Y.F. The impact of high temperature on mechanical properties and behaviors of sandstone. *Front. Earth Sci.* **2024**, *12*, 1322495. [CrossRef]
9. Zhao, J.; Guo, Y.; Chen, P.S.; Hu, L.; Wang, J.R. True Triaxial Shear Strength and Failure Mechanism of Sandstone Under Real-Time High-Temperature Conditions. *Rock Mech. Rock Eng.* **2025**, *58*, 6211–6231. [CrossRef]
10. Dong, C.L.; Fan, C.T.; Lu, X.Y.; Zhao, G.M.; Qi, M.J.; Qin, R.P. Mechanical and Energy Evolution Characteristics of Sandstone Under True Triaxial Cyclic Loading. *Appl. Sci.* **2023**, *13*, 7230. [CrossRef]
11. Li, J.Y.; Liu, D.Q.; He, M.C.; Yang, J.S. Excess energy characteristics of true triaxial multi-faceted rapid unloading rockburst. *J. Cent. South Univ.* **2024**, *31*, 1671–1686. [CrossRef]
12. Zhang, R.J.; Liu, Y.R.; Zhu, L.; Hou, S.K.; Li, Z.; Zhao, T.; Chen, X. Failure characteristics and energy evolution process of delayed and instantaneous basalt rockburst under true triaxial conditions. *Int. J. Rock Mech. Min. Sci.* **2024**, *183*, 105909. [CrossRef]
13. Eberhardt, E.; Stead, D.; Stimpson, B.; Read, R.S. Identifying crack initiation and propagation thresholds in brittle rock. *Can. Geotech. J.* **1998**, *35*, 222–233. [CrossRef]

14. Chen, L.; Dong, J.S.; Guo, L.J.; Li, Q.W.; Qiao, L. Multi-Parameter acoustic emission precursory information and failure early-warning strategies for high-strength rrittle rock. *Earth Sci.* **2024**, 1–18. Available online: https://link.cnki.net/urlid/42.1874.P.20260519.1053.012 (accessed on 24 April 2026).
15. Wang, Z.P.; Gu, Y.L.; Geng, W.B.; Fang, J.; Liao, S. Laboratory study on AE count fractal feature of sandstone acoustic emission with different granularity. *Chin. J. Undergr. Space Eng.* **2018**, *14*, 594–599.
16. Wang, K.Y.; Luo, G.J.L.Z.Y.; Gao, J.Q.; Xu, Y.D.; Li, S.L. Study on the effect of heterogeneity on the macro and mesoscopic failure characteristics of sandstone samples. *Chin. J. Rock Mech. Eng.* **2023**, *42*, 391–402.
17. Li, G.; Wu, X.F.; Yang, Y.; Feng, J.X.; Li, H.T. Mesoscopic fracture simulation of dense sandstone based on acoustic emission. *J. Civ. Environ. Eng.* **2025**, *47*, 125–134.
18. Cao, J.; Zhang, C.J.; Ren, J.H.; Li, X.L. Study on Fracture-Damage Mechanical Mechanism and Mesoscopic Simulation of Deep Sandstone. *Met. Mine* **2024**, *580*, 69–75.
19. Yu, J.; Chen, S.J.; Chen, X.; Zhang, Y.Z.; Cai, Y.Y. Experimental investigation on mechanical properties and permeability evolution of red sandstone after heat treatments. *J. Zhejiang Univ. Sci. A* **2015**, *16*, 749–759. [CrossRef]
20. Yin, T.B.; Li, X.B.; Xia, K.W.; Huang, S. Effect of Thermal Treatment on the Dynamic Fracture Toughness of Laurentian Granite. *Rock Mech. Rock Eng.* **2012**, *45*, 1087–1094. [CrossRef]
21. Gao, M.B.; Li, T.B.; Wei, T.; Meng, L.B. A statistical constitutive model considering deterioration for brittle rocks under a coupled thermal-mechanical condition. *Geofluids* **2018**, *2018*, 3269423. [CrossRef]
22. Zhang, H.W.; Wan, Z.J.; Zhou, C.B.; Zhao, Y.X.; Wang, W.; Yang, Y.L.; Teng, T. High temperature mechanical properties and thermal shock effect of hot dry rock. *J. Min. Saf. Eng.* **2021**, *38*, 138–145.
23. Gao, M.B.; Li, T.B.; Zhang, L.; Gao, Y.; He, Z.H.; Zhong, Y.Y. Fracture mechanism and constitutive model considering post-peak plastic deformation of marble under thermal–mechanical action. *Geomech. Geophys. Geo-Energy Geo-Resour.* **2024**, *10*, 168. [CrossRef]
24. Li, T.B.; Meng, L.B.; Wang, L.S. *Stability of High In-Situ Stress Tunnels and Prevention of Rockburst and Large Deformation Disasters*; Science Press: Beijing, China, 2016.

Disclaimer/Publisher's Note: The statements, opinions and data contained in all publications are solely those of the individual author(s) and contributor(s) and not of MDPI and/or the editor(s). MDPI and/or the editor(s) disclaim responsibility for any injury to people or property resulting from any ideas, methods, instructions or products referred to in the content.